Hindawi
Shock and Vibration
Volume 2021, Article ID 6547213, 12 pages
https://doi.org/10.1155/2021/6547213

*Research Article*

# Effects of Heat Treatment on the Microstructure and Mechanical Properties of Selective Laser Melting 316L Stainless Steel

**Jingfa Lei**,[1,2] **Yongsheng Ge**,[1] **Tao Liu**,[1,2] **and Zhan Wei**[1]

[1]*School of Mechanical and Electrical Engineering, Anhui Jianzhu University, Hefei, China*
[2]*Anhui Education Department Key Laboratory of Intelligent Manufacturing of Construction Machinery, Hefei, China*

Correspondence should be addressed to Tao Liu; tao.liu@ahjzu.edu.cn

Received 16 April 2021; Revised 30 September 2021; Accepted 8 October 2021; Published 20 October 2021

Academic Editor: Guoda Chen



316L stainless steel materials are widely used in impact-resistant structures. Heat treatments could affect the mechanical properties of 316L stainless steel parts formed by selective laser melting (SLM), which is vital for ensuring service safety. This study aimed to analyze the mechanical behavior of SLM 316L stainless steel under different heat treatment methods. Therefore, test specimens were prepared using the SLM technique and then annealed at 400°C for 1 h. The solution was treated at 1050°C for 20 min. The dynamic compressive mechanical properties of the deposited, annealed, and solution-treated specimens were tested at high strain rates by using a split Hopkinson pressure bar (SHPB) experimental apparatus. Moreover, the microstructures of the previously mentioned samples were analyzed by optical microscopy and scanning electron microscopy. The experimental results showed that the three-state samples exhibited strain rate sensitivity in the dynamic mechanical tests and that solution treatment could alter their mechanical properties significantly. In addition, the microstructure of the deposited specimens presented cylindrical cellular crystal features, which have a higher dislocation density. Hence, the yield strength of deposited specimens is higher than that of the solution-treated ones. After annealing, the microstructures of the samples did not change obviously, and their dynamic yield strength remained almost unchanged. After solution treatment, its cellular crystal disappeared and dislocation density dropped dramatically, resulting in a sharp decrease in yield strength. Finally, this research can provide a theoretical reference for broadening the practical application of SLM 316L material parts.

## 1. Introduction

Selective laser melting (SLM) is one of the essential technologies in the field of additive manufacturing (AM). The metal parts formed directly by the technique exhibit high dimensional accuracy, good surface quality, and almost 100% density [1–3]. SLM 316L stainless steel, as a typical AM metal, is widely used in the aerospace and marine machinery fields due to its good mechanical properties [4–8]. The metal components of the SLM 316L stainless steel are often subjected to harsh service conditions during use, requiring higher demands on their mechanical properties. However, the mechanical properties of SLM 316L stainless steel vary considerably after heat treatment methods [9, 10]. Therefore, it is essential to clarify the effect of heat treatment on the dynamic mechanical properties of SLM 316L stainless steel for ensuring its service performance.

At present, extensive studies have been conducted on the microstructure and mechanical properties of SLM 316L stainless steel. Salman et al. [11] studied the microstructure and quasistatic tensile properties of SLM 316L stainless steel at different annealing temperatures and found that tensile strength decreased with increasing temperature. Kong et al. [12] researched the microstructure and mechanical properties of SLM 316L stainless steel at different solution temperatures and determined that yield strength decreased with rising temperature. Tascioglu et al. [13] investigated the effects of heat treatment on the microstructure and wear behavior of SLM 316L stainless steel. They found that the effect of porosity on wear behavior was more dominant than that of microhardness. Wang et al. [14] compared the yield

strength and tensile toughness of 316L stainless steel specimens prepared via SLM and casting. The results showed that the tensile mechanical properties of SLM 316L stainless steel were better than those of the conventional cast stainless steel. Based on the previously mentioned literature, the mechanical properties of SLM 316L stainless steel have been comprehensively investigated. However, there are few studies on the dynamic compressive mechanical properties of SLM 316L stainless steel.

Therefore, the microstructure and dynamic mechanical properties of SLM 316L stainless steel after different heat treatments were investigated in this work. Test samples formed by SLM were annealed at 400°C for 1 h and solution treated at 1050°C for 20 min. The dynamic compressive mechanical properties of the deposited, annealed, and solution-treated samples were tested by a split Hopkinson pressure bar (SHPB) experimental device at strain rates of 1000, 2000, and 3000 $s^{-1}$. The microstructures of the previously mentioned samples were analyzed via optical microscopy and scanning electron microscopy. The microscopic mechanism of the heat treatments on dynamic compressive mechanical properties was investigated to provide a theoretical reference for ensuring its service performance and broadening the application of SLM 316L stainless steel.

## 2. Experimental Materials and Methods

*2.1. Preparation of Experimental Materials and Samples.* Test specimens were prepared using an SLM machine called iSLM280, equipped with a 200 W fiber laser and a high-precision laser scanning system. The 316L stainless steel powder used for the machine was prepared by gas atomization, and its microscopic morphology is shown in Figure 1. The powder has good sphericity and fluidity, with a particle size distribution ranging from 15 $\mu$m to 53 $\mu$m. The chemical compositions of this powder are listed in Table 1 [15, 16].

According to the experimental requirements, two kinds of cylindrical specimens were fabricated. The quasistatic test specimens were designed as cylindrical specimens with a diameter of 12 mm and a height of 15 mm according to the standard of GB/T 7314-2017. The compression test of metallic materials was conducted at room temperature. The dynamic test specimens were designed as cylindrical specimens with a diameter of 12 mm and a height of 5 mm, based on the requirement of the L/D (length/diameter) ratio in the range of 0.3–0.8. The process parameters used to form the specimens are given in Table 2. In addition, the alternating stripes scanning strategy was used for the forming process (Figure 2). Each layer was scanned using simple alternating scan vectors, and the scanning direction rotated 90° after each layer [17, 18].

*2.2. Experimental Methods*

*2.2.1. Heat Treatment and Microstructure Observation.* The heat treatments of the specimens were carried out in a vacuum tube heat-treatment furnace called BTF-1200C–S-25-90, and the tube was required to be evacuated to isolate the air before the experiment. The following two heat treatment methods were adopted in this paper. Stress relief annealing raised the temperature to 400°C at a rate of 10°C/min and then maintained this temperature for 1 h. After that, the specimens were cooled in the furnace to 200°C and then taken out to be air-cooled to room temperature (25°C). The solution treatment was carried out at a rate of 10 °C/min to 400°C. Then, the temperature was rapidly increased to 1050°C at a rate of 10°C/s, held for 20 min. Finally, the specimens were cooled to room temperature by water cooling. The specific heat treatment process is summarized in Table 3.

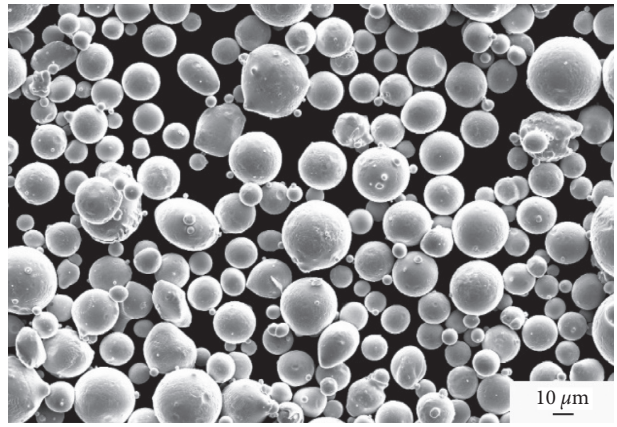


Figure 1: Microstructure of SLM 316L stainless steel powder.

Table 1: Chemical components of 316L stainless powder (mass, %).

| Element | C | Cr | Mn | Mo | Ni | Fe |
|---|---|---|---|---|---|---|
| Mass (%) | 0.022 | 17.16 | 1.45 | 2.71 | 12.2 | Bal. |

The treated specimens were divided into three groups based on state: deposited, annealed, and solution-treated. The observation surface of the specimen was mechanically polished to obtain a bright mirror surface with good reflectivity. Then, the specimens were etched with aqua regia solution (3 mL HCL + 1 mL $HNO_3$) for 6-10 s to produce metallographic specimens. The microstructural morphology of the specimens and their elemental distribution were analyzed under a Zeiss 40MAT inverted optical microscope and a Zeiss EVO180 scanning electron microscope, respectively.

*2.2.2. Testing of Dynamic Mechanical Properties.* Quasistatic compression experiments tests were carried out on 316L stainless steel specimens ($12 \times 15\ mm^2$) in three states at room temperature (25°C) by using the MTS Landmark® 370.5 electrohydraulic servo experimental system (Figure 3). The specimens were fixed at the center of the base, and lubricant was applied at the contact surfaces to reduce the end friction; thus, the specimens were ensured in a unidirectional force state. An external tensiometer was added to the equipment to ensure the accuracy of the experimental results. Moreover, three sets of experiments were

Table 2: Technology parameters of 316L stainless steel by SLM processing.

| Laser power (W) | Scan speed (mm/s) | Layer thickness ($\mu$m) | Hatch spacing (mm) |
|---|---|---|---|
| 200 | 1000 | 50 | 0.1 |

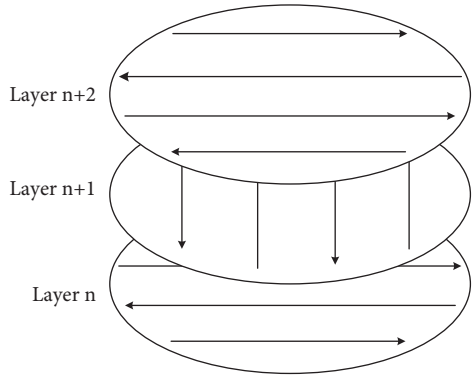


Figure 2: Schematics representing the alternating stripes scanning strategy.

Table 3: The heat treatment process of 316L stainless steel produced via SLM.

| Number | Heat treatment process | Cooling method |
|---|---|---|
| I | Deposited | — |
| II | Stress relief annealing at 400°C for 1 h | Air cooling |
| III | Solution treatment at 1050°C for 20 min | Water cooling |

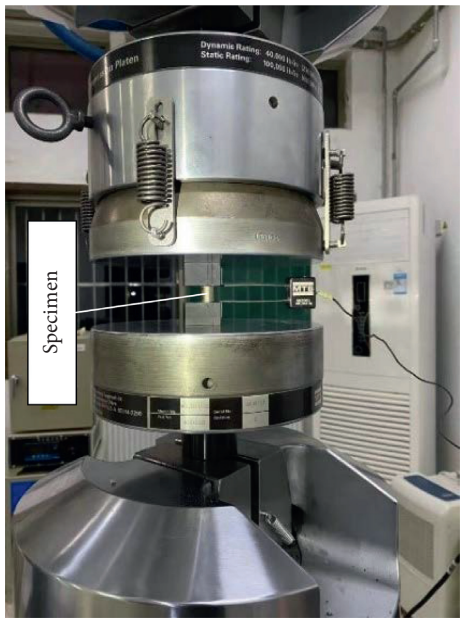


Figure 3: Quasistatic compression experiments.

repeated for each state specimen. According to the specimen size, the chunk loading speed was set to 0.015 mm/s, and the control strain rate was 0.001 $s^{-1}$.

The SHPB experimental apparatus was used to perform dynamic compression mechanical experiments at high strain rates. This apparatus consists of a loading device (air gun), compression bar system (impact, incidence, and transmission bar), data acquisition system, and damping absorber, as shown in Figure 4 [19, 20]. The material of each bar was low alloy steel with an elastic modulus of 210 GPa, density of 7.83 g/$cm^3$, and wave speed of 5100 m/s.

The SLM 316L stainless steel cylindrical specimen ($\varphi 12 \times 5\ mm^2$) was clamped between the incident and transmission bar. The lubricant was applied to the contact area at both ends of the specimen to reduce the end-face friction effect. The air gun pushes the impact bar to strike the incident bar. The process generates a one-dimensional (1D) stress wave $\sigma_i$ transmitted through the specimen to the transmission bar. When the stress wave passes through the specimen, part of the stress wave is reflected into the incident bar, forming the reflected stress wave $\sigma_r$, and the rest is transmitted into the transmission bar, forming the transmitted stress wave $\sigma_t$. The three stress waves generated elastic strain $\varepsilon_i$, $\varepsilon_r$, and $\varepsilon_t$ in the incident and transmitted bars, respectively. Then, the strain rate $\dot{\varepsilon}(t)$, strain $\varepsilon(t)$ , and stress $\sigma(t)$ were obtained by calculating the strain signal through (1). Afterward, the data is transformed into a stress-strain curve through data processing [21, 22]:

$$\begin{cases} \dot{\varepsilon}(t) = \dfrac{c_0}{L_0}\left(\varepsilon_i - \varepsilon_r - \varepsilon_t\right), \\ \varepsilon(t) = \dfrac{c_0}{L_0}\displaystyle\int_0^t \left(\varepsilon_i - \varepsilon_r - \varepsilon_t\right)\mathrm{d}t, \\ \sigma(t) = \dfrac{A}{2A_0}E\left(\varepsilon_i + \varepsilon_r + \varepsilon_t\right), \end{cases} \tag{1}$$

where $c_0$, $E$, and $A$ are the elastic wave velocity, elastic modulus, and cross-sectional area of the compression bar and $L_0$ and $A_0$ are the length and cross-sectional area of the specimen.

## 3. Experimental Results and Analysis

*3.1. Microstructure and EDS Analysis.* Figure 5 displays the microstructure of the deposited SLM 316L stainless steel and its EDS analysis. There are many cellular structures in the specimen, polygonal in the transverse section and parallel boundaries along the longitudinal section, in Figures 5(a) and 5(b). Thus, the three-dimensional view of the cellular structure is similar to a honeycomb along the temperature gradient, as shown in Figure 5(c). Depending on the observation direction, the morphology of the cellular structure is different [23]. It can be a circle, ellipse, or two parallel lines. Moreover, the diameter (width) of individual tiny

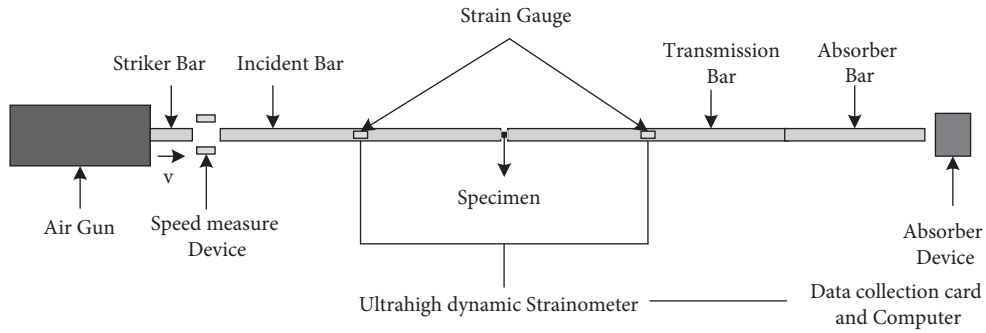


Figure 4: Schematic of the SHPB experimental device.

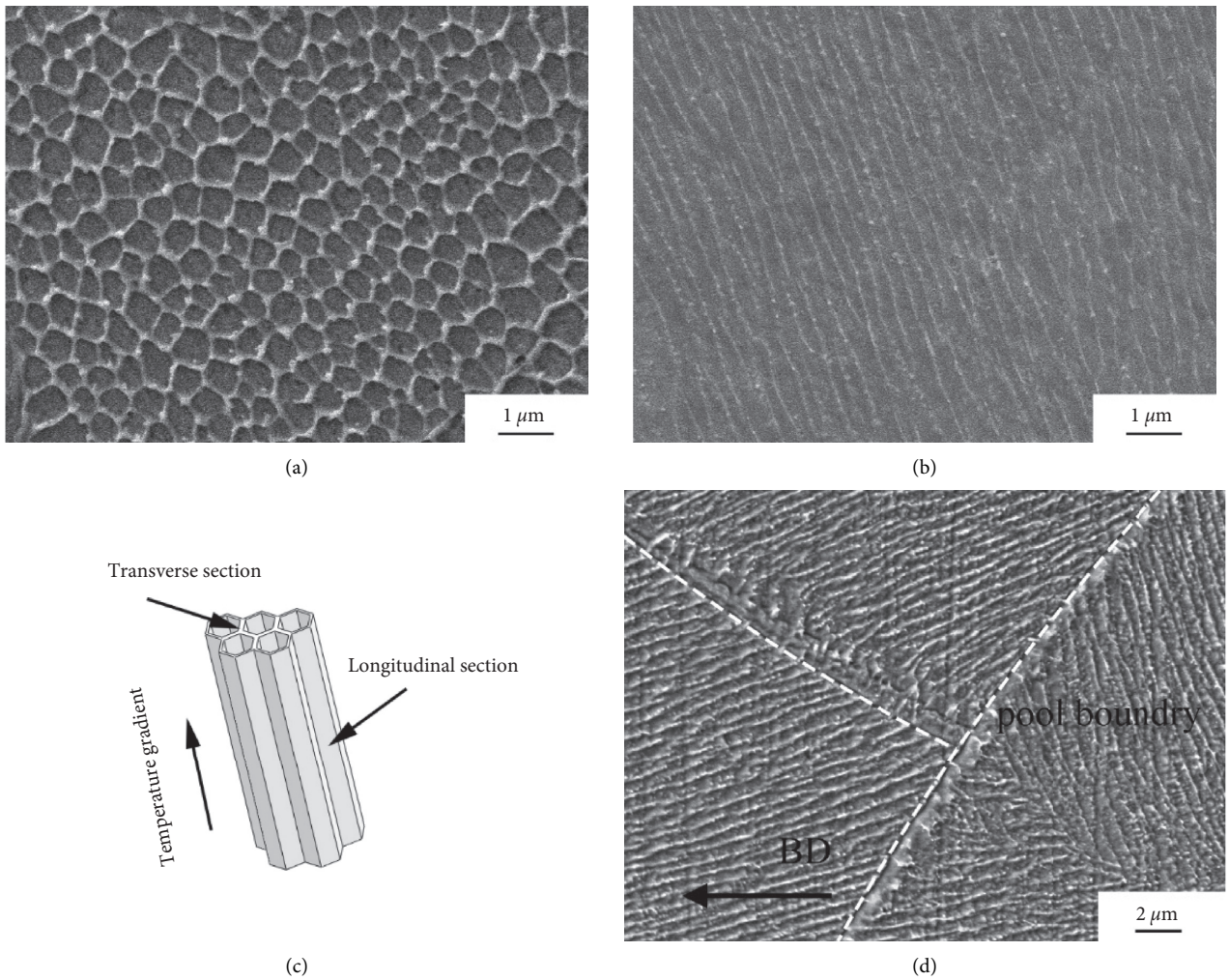


Figure 5: Continued.

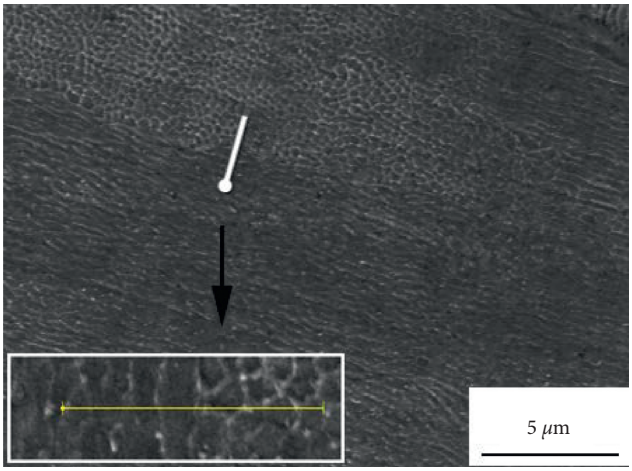


(e)

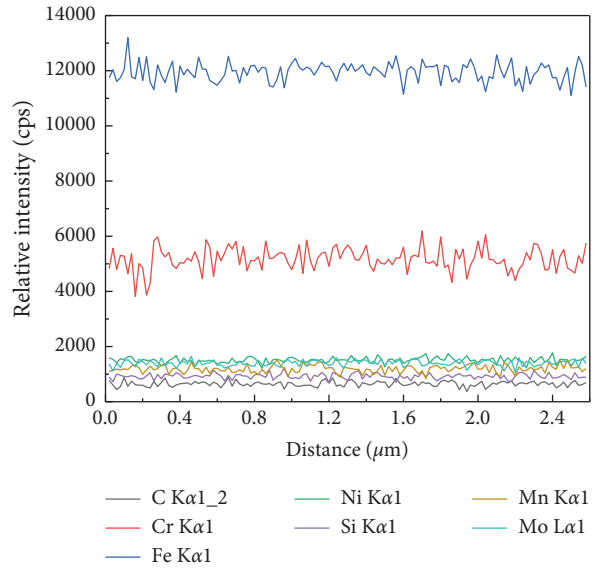


(f)

FIGURE 5: Microstructure and EDS analysis of the deposited SLM 316L stainless steel samples. (a) Transverse section of a cellular structure, (b) longitudinal section of a cellular structure, (c) three-dimensional view of cellular structure, (d) growth direction of cellular crystal between adjacent molten pool boundaries, (e) scope of the EDS line scan, and (f) elemental analysis of the EDS line scan.

crystals was measured to be approximately 0.5 $\mu$m [24, 25]. Meanwhile, Figure 5(d) illustrates the typical direction of honeycomb crystal growth between adjacent pool boundaries along the building direction. The cell growth in the adjacent regions is highly variable and presents a random distribution.

Moreover, EDS characterized the element content at the subgrain boundaries. At the given length scale (Figure 5(e)), the results show that there is no obvious change in the content of each element (Figure 5(f)). However, the relevant literature pointed that Cr and Mo were enriched at the subgrain boundaries; there is about 2 wt% more Cr content at the subgrain boundary, and the Mo content was approximately 1.7 times higher at the subgrain boundary [26]. Combined with the experimental results, the analysis in this paper suggests that the grain boundaries of SLM 316L stainless steel have elements enrichment. However, the change of contents is too low to reflect in the graph.

The analysis indicates that the honeycomb crystal structure was produced by the unique processing method of SLM. In general, temperature gradient (G) and crystal growth rate (R) play a key role in determining the solidification morphology, and a high G/R ratio leads to the formation of cellular structures [27]. SLM, a rapid additive manufacturing technique, has a fast cooling rate of the metal solute that generates extremely high-temperature gradients. This solidification method promotes the growth of micron-sized cellular structures and causes them to exhibit a honeycomb arrangement. Moreover, the honeycomb structures occur by epitaxial growth. The crystal orientation of the previous layer is closely related to the heat flow direction of the next layer, which suggests that the base layer plays the leading role in the growth direction of the cellular structure [28]. However, the heat flow direction in the nonuniform temperature field is usually random during the SLM forming process, so the cellular growth direction is randomly distributed.

Figure 6 shows the microstructure of annealed SLM 316L stainless steel and its EDS analysis. In Figures 6(a) and 6(b), the cellular structure is still present in the annealed tissue with a polygon in the transverse section and the parallel boundary along the longitudinal section, showing the same honeycomb arrangement as the deposited state specimens. Furthermore, the diameter (width) of individual cellular grain remains at approximately 0.5 $\mu$m. In Figure 6(c), the growth direction of this honeycomb structure is diverse at the adjacent pool boundaries, showing a random distribution along the building direction. Similarly, EDS analysis was performed at the subgrain boundaries. The element occupancy remains essentially the same as that of the deposited state specimens. The analytical ranges are shown in Figure 6(d) and the results in Figure 6(e).

It can be concluded that the microscopic morphology of the annealed specimens and their elements composition did not change significantly compared with the deposited specimens. The cellular structure in SLM metals tends to decompose after high-temperature treatment due to nonequilibrium solidification, similar to other substable structures. However, the cellular structure is thermally stable at high temperatures, owing to this relatively low stored energy [29]. The analysis reveals that stress relief annealing at a constant temperature of 400°C is not sufficient to break the stability of the cellular structure. This temperature is not reaching the phase transformation point of the austenitic crystals. The cellular structure cannot decompose, and the tissue does not recrystallize and coarsen. Therefore, the

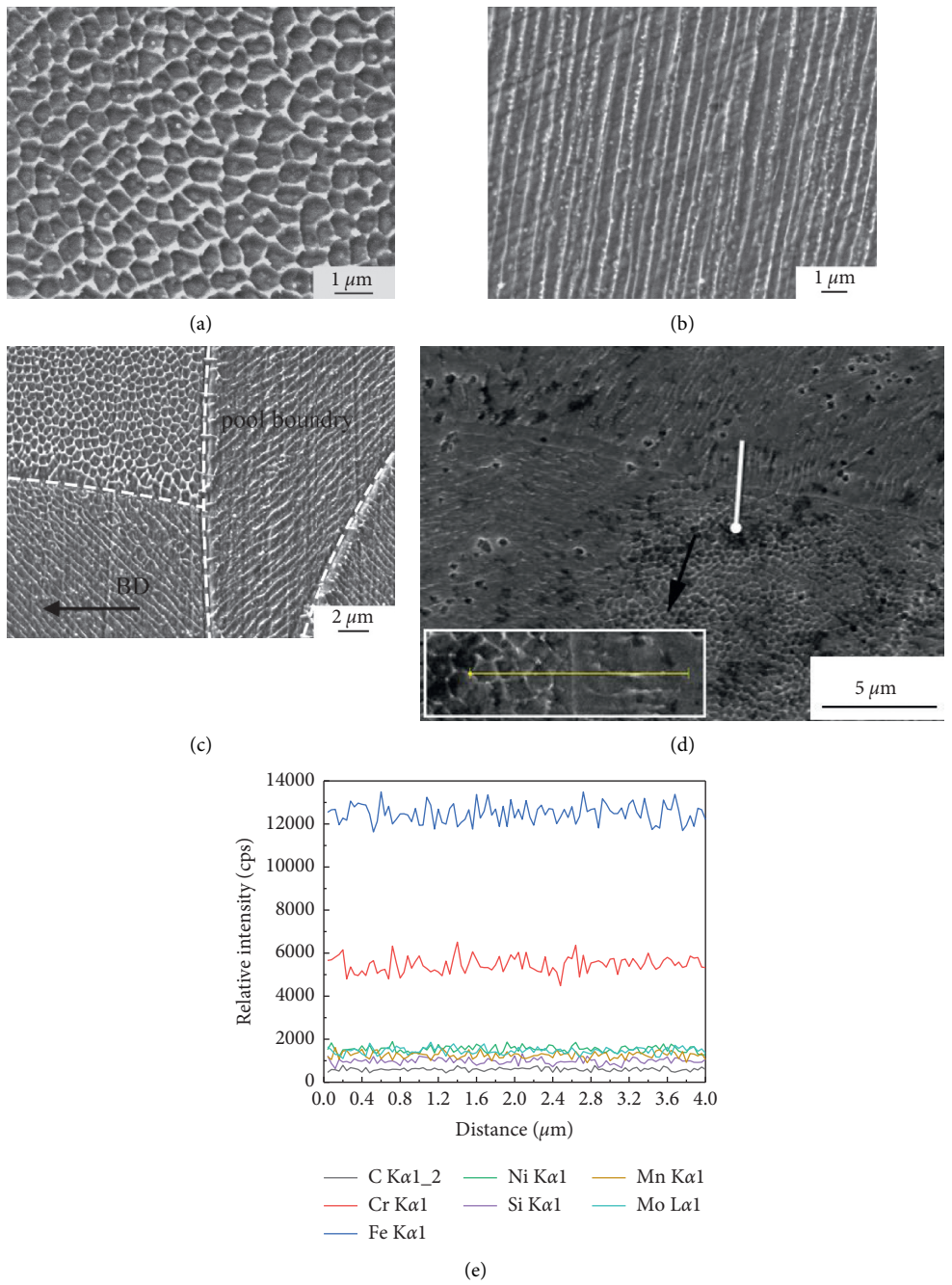


Figure 6: Microstructure and EDS analysis of the annealed SLM 316L stainless steel. (a) Transverse section of a cellular structure, (b) longitudinal section of a cellular structure, (c) growth direction of cellular crystal between adjacent molten pool boundaries, (d) scope of the EDS line scan, and (e) elemental analysis of the EDS line scan.

anisotropic cellular structure still exists in the annealed microstructure. Consequently, the morphology of the annealed tissue and its elements content remains unchanged.

The microstructural morphology and EDS analysis of the specimens after solution treatment at 1050°C for 20 min are shown in Figure 7. The typical cellular structure features disappeared, as displayed in Figures 7(a) and 7(b); however, other crystalline structures can be observed, with individual grain sizes varying from 10 $\mu$m to 40 $\mu$m. The change of microsize indicates that the anisotropic honeycomb cellular structure decomposed after the solution treatment. Moreover, a mass of nanosized particles precipitated out and was extensively present at the grain boundaries, as shown in Figure 7(c), similar to other literature studies [30]. Furthermore, the scanning analysis of grain boundaries and interiors found no significant differences in the alloying element composition of the specimens within the measurement range (Figures 7(c) and 7(d)). It can be seen that there is no phase transformation of SLM 316L stainless steel after heat treatment.

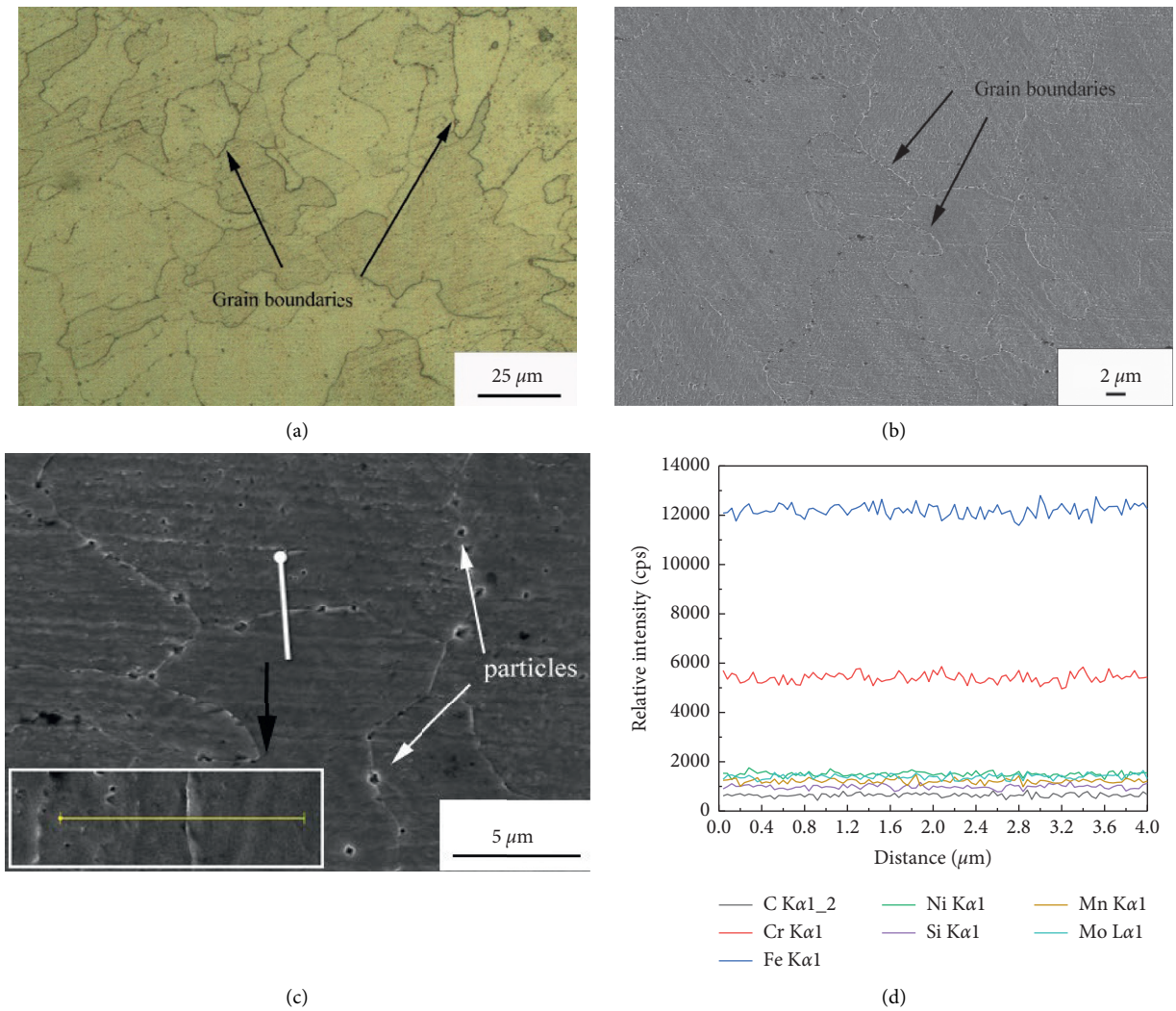


FIGURE 7: Microstructure and EDS analysis of the solution-treated SLM 316L stainless steel. (a) Grain boundary under OM, (b) grain boundary under SEM, (c) scope of the EDS line scan, and (d) elemental analysis of the EDS line scan.

The analysis shows that the solution heat treatment temperature of 1200°C breaks the thermal stability of the honeycomb structure, and the subboundaries of the cellular grains melt away. Therefore, there is no local morphological difference in the solution-treated 316L stainless steel in the solution microstructure due to the disappearance of the cellular structure. At the same time, the higher holding temperature achieves the environmental condition required for austenite nucleation and coarsen. The cellular structure melts, and the austenite grains grow, forming a large coarsening structure in the microscopic region. In addition, after solution treatment, the specimens formed an equiaxed austenite structure, which was different from the other two specimens. Based on the previously mentioned analysis, the change in microscopic dimensions of solution-treated 316L stainless steel will definitely lead to a change in mechanical properties.

*3.2. Analysis of Dynamic Mechanical Properties.* The reliability of the SHPB experimental technique should satisfy the 1D stress wave assumption and homogeneity assumption [31]. For $\varphi$14.5 mm thin straight bar system, the 1D stress wave assumption holds. The calculated incident + reflect (In + Re) curve largely coincides with the collected transmission curve (Figure 8), indicating that the test materials achieved stress balance throughout the loading process.

The quasistatic stress-strain curves of the three state specimens at a strain rate of 0.001 $s^{-1}$ are shown in Figure 9. Each curve can be divided into elastic and plastic phases, but no evident yield platform was found. When the strain is below 0.02, the stress shows a linear growth with elastic deformation; it is a typical linear elastic characteristic of most metal materials. At the plastic phase, no evident yielding phenomenon was observed in the graphs. However, the slope of the curve changes obviously, which indicates that the material is subject to the combined effect of strain strengthening while yielding occurred. This phenomenon is commonly found in quasistatic compression experiments of plastic materials. When the curve entered the stable-strengthened stage, its stress gradually increased with the plastic deformation, exhibiting strain strengthening characteristics of the specimens.

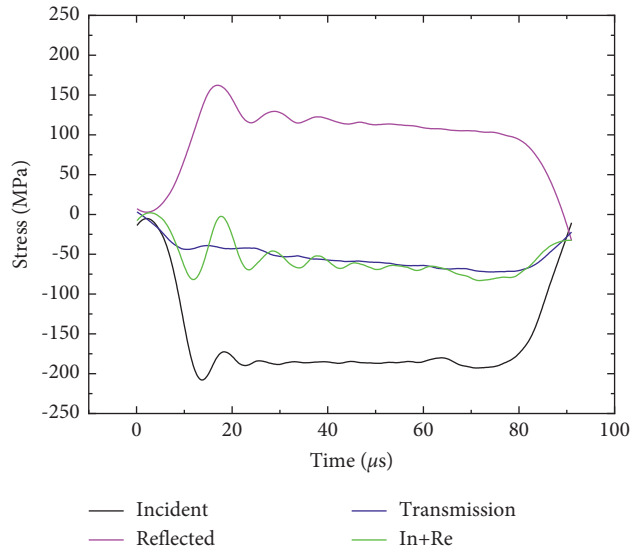


Figure 8: Diagram of the stress-time curve.

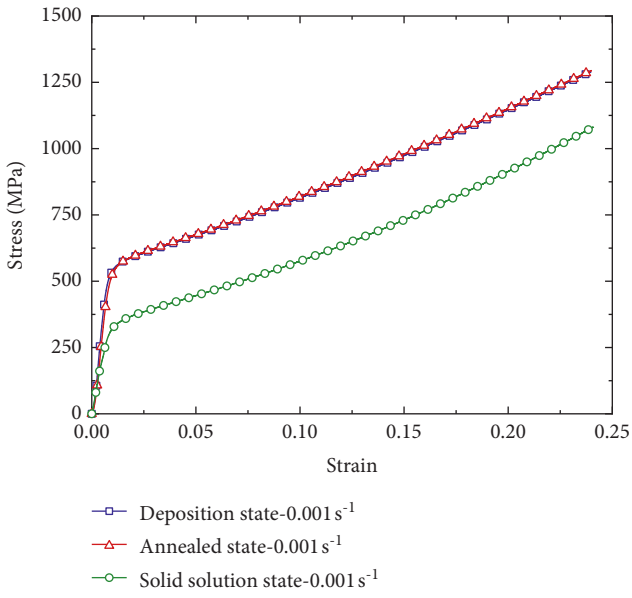


Figure 9: Quasistatic compressive stress-strain curve.

The stress-strain curves obtained from the dynamic compression tests are shown in Figures 10(a)–10(c). Dynamic mechanical properties were analyzed by comparing with the quasistatic ($0.001\ s^{-1}$) curves. The curves at high strain rates exhibit similar characteristics to the quasistatic state and can be similarly divided into elastic and plastic phases [32]. Moreover, compared with the quasistatic experimental curves, the yield strength of the specimen increased by an average of 50.65% when the loading strain rate was increased from 0.001 to $1000\ s^{-1}$ (the deposited specimens increased by 51.60%, the annealed specimens increased by 48.67%, and the solution-treated specimens increased by 51.68%). It indicates that the material has a significant strain rate strengthening behavior in dynamic mechanical tests. However, when the strain rate was increased from 1000 to $3000\ s^{-1}$, the yield strength increased slightly, only about 17.81% (the deposited specimen increased by 15.95%, the annealed specimen increased by 18.01%, and the solution-treated specimen increased by 19.47%). This finding strongly confirmed that SLM 316L is a typical strain-rate sensitive material and has strain rate strengthening properties. However, this strain-rate sensitivity was not exhibited significantly in the high strain rate range.

Table 4 provides the peak yield stresses of the deposited, annealed, and solution-treated 316L specimens in the quasistatic and dynamic mechanics experiments. The effect of heat treatment on mechanical properties is analyzed by comparing at the same strain rate.

As indicated in Table 4, the solution heat treatments significantly affected the mechanical properties of 316L stainless steel. The yield strength of specimens decreased slightly after stress relief annealing when compared under the same strain rate conditions (with a decrease of 2.11% at $0.001\ s^{-1}$, 3.66% at $1000\ s^{-1}$, 7.21% at $2000\ s^{-1}$, and 1.43% at $3000\ s^{-1}$). However, the yield strength of specimens decreased significantly after solid solution treatment (with a decrease of 37.21% at $0.001\ s^{-1}$, 35.94% at $1000\ s^{-1}$, 34.93% at $2000\ s^{-1}$, and 35.49% at $3000\ s^{-1}$). From the analysis, it can be concluded that the solution heat treatment can reduce the yield strength and enhance the plasticity of SLM 316L stainless steel. Furthermore, according to Figure 10(c), the solution-treated samples have a more considerable plastic deformation in the dynamic tests, which indicates that the samples have a higher toughness.

## 4. Discussion

Following the primary experimental data, SLM 316L stainless steel specimens exhibit different mechanical behavior in mechanical tests after heat treatment.

The main factors affecting the mechanical properties were identified by characterizing the microstructure of

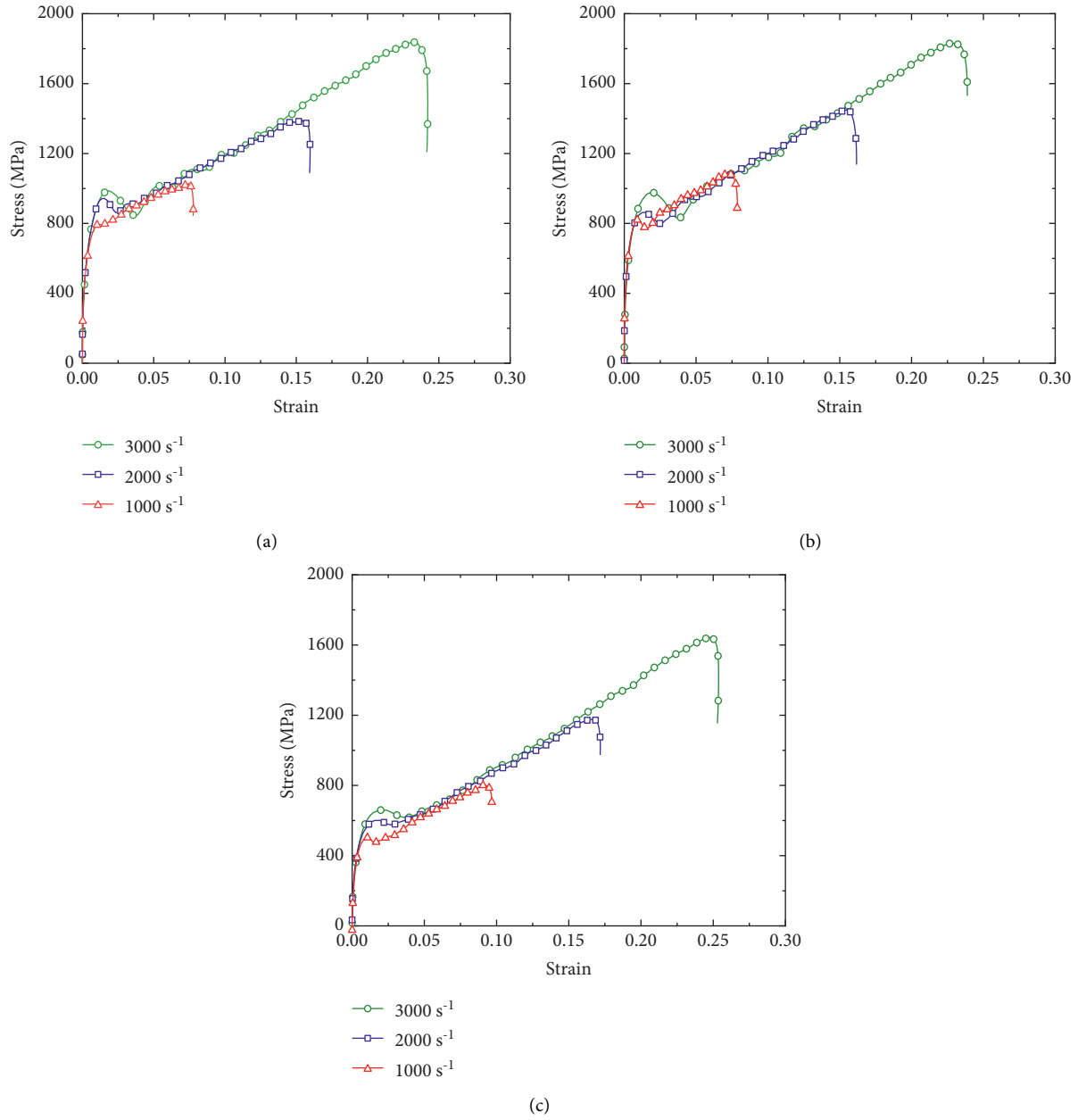


Figure 10: Dynamic stress-strain curve. (a) Deposited state, (b) annealed state, and (c) solution-treated state.

Table 4: The trend of the peak yield stress (stress, MPa).

| Sample status strain rate (s) | Deposited state | Annealed state | Solution-treated state |
|---|---|---|---|
| $0.001^{-1}$ | 544.64 | 533.12 | 334.75 |
| $1000^{-1}$ | 822.78 | 792.62 | 507.75 |
| $2000^{-1}$ | 924.42 | 857.80 | 558.17 |
| $3000^{-1}$ | 954.02 | 940.33 | 606.63 |

deposited, annealed, and solution-treated specimens. The cellular structure can lead to substantial differences in the mechanical properties of SLM specimens, significantly increasing the yield strength. The microstructure of the deposited specimens is characterized by a honeycomb structure composed of cellular crystals, and the size of each grain is about 0.5 $\mu$m. Studies in the relevant literature have concluded that this closely spaced honeycomb structure can produce large dislocation density in its organization , which undoubtedly leads to differences in mechanical properties of samples. When the material is deformed, the dislocation capability of the grains along the grain boundaries is

hindered [33, 34], resulting in the high yield strength. This phenomenon is called grain strengthening. Therefore, the dynamic mechanical properties of the deposited specimens are superior to those of the heat-treated specimens. However, in this state, the specimen organization is not homogeneous and has significant residual stresses that may lead to instability in their mechanical properties during use [35, 36].

After stress relief annealing at 400°C for 1 h, the size of the cellular structure and its anisotropic orientation did not change obviously. Dislocation density between microstructures was unchanged, and the intergranular strengthening phenomenon did not improve. So, the dynamic yield strength did not exhibit a significant downward trend. However, stress relief annealing eliminated the residual stresses remaining in the SLM process, affecting the later processing and use of the formed parts. Therefore, stress relief annealing is an ideal heat treatment method that can ensure high-strength mechanical properties and improve the service performance of materials [37]. After solution treatment at 1050°C for 20 min, the cellular structure with different orientations disappeared, and coarsened austenite grains appeared. At this moment, the size of the microstructure increased from 0.5 $\mu$m to 15-40 $\mu$m, and the dislocation density decreases with grain coarsening during solution treatment. The weakening of the resistance to dislocation slip leads to the low yield strength of the specimens. However, the specimens under this heat treatment method exhibited good toughness and plasticity, improving the machinability of SLM metals [38, 39].

In summary, this study investigates the effects of heat treatment on the static and dynamic mechanical properties of SLM 316L stainless steel, providing a theoretical reference to the service performance of SLM 316L stainless steel and broadening the application range of SLM 316L stainless steel. However, the dynamic mechanical properties of SLM 316L stainless steel metal components are only a part of their comprehensive performance. Therefore, this is not enough to provide a deeper understanding of the other excellent properties. In this regard, research on the quantitative description of residual stresses in SLM 316L stainless steel and the relationship between its mechanical properties is a good direction for further study.

## 5. Conclusions

This study investigated the microstructure of SLM 316L stainless steel in the deposited, annealed, and solution-treated states and its dynamic compression mechanical properties. It analyzed the effects of different heat treatments on the dynamic compression mechanical properties of SLM 316L stainless steel through its microscopic mechanisms. Based on the results, the following conclusions can be drawn:

(1) The microstructure of the deposited SLM 316L stainless steel sample is mainly composed of columnar cells with different growth directions, exhibiting the characteristics of a honeycomb arranged structure. After stress relief annealing for 1 h at 400°C, the morphology of the annealed microregion did not change significantly, and the cellular crystal structure still existed. At 1050°C for 20 min solution treatment, the cellular crystal organization of the specimen disappeared, and the coarsened austenite organization can be observed.

(2) The yield strength of the deposited specimens tended to be the highest among the three specimens due to the high dislocation density of the submicron cellular grain structure formed during SLM. In this state, the specimen organization is not homogeneous and has significant residual stresses that may lead to instability in their mechanical properties. After stress relief annealing at 400°C for 1 h, the microstructure of the annealed specimens did not change significantly, and yield strength tended to decrease slightly. Moreover, this heat treatment can considerably increase the serviceability of the material without changing its high-strength properties. After solution treatment at 1050°C for 20 min, the cellular grain structure grew and formed coarse austenite grains. The significant dislocation density reduction leads to a sharp decrease in the yield strength, which is good for improving the machinability of SLM metal materials.

## Data Availability

The data used to support the findings of this study are available from the corresponding author upon request.

## Conflicts of Interest

The authors declare that they have no conflicts of interest regarding the publication of this paper.

## Acknowledgments

This research was supported by Hefei Municipal Natural Science Foundation (no. 2021019), Anhui Education Department Top-Notch Talents Academic Funding Project (no. gxbjZD2020078), and Anhui Education Department Excellent Young Talent Support Project (no. gxyqZD2019057).

## References

[1] A. Tawfik, M. Radwan, A. Attia, P. Bills, R. Racasan, and L. Blunt, "The detection of unfused powder in EBM and SLM additive manufactured components," *International Journal of Automation Technology*, vol. 14, no. 6, 2020.

[2] W. Zhai, W. Zhou, S. M. L. Nai, and J. Wei, "Characterization of nanoparticle mixed 316 L powder for additive manufacturing," *Journal of Materials Science & Technology*, vol. 47, pp. 162–168, 2020.

[3] L. Zhou, S. Feng, M. Sun, B. Xu, and D. Li, "Interfacial microstructure evolution and bonding mechanisms of 14YWT alloys produced by hot compression bonding," *Journal of Materials Science & Technology*, vol. 35, no. 8, pp. 1671–1680, 2019.

[4] K. P. Karunakaran, S. Suryakumar, V. Pushpa, and S. Akula, "Low cost integration of additive and subtractive processes for hybrid layered manufacturing," *Robotics and Computer-Integrated Manufacturing*, vol. 26, no. 5, pp. 490–499, 2010.

[5] K. C. Bae, K. S. Ha, Y. H. Kim, J.-J. Oak, W. Lee, and Y. H. Park, "Building direction dependence of wear resistance of selective laser melted aisi 316l stainless steel under high-speed tribological environment," *International Journal of Advanced Manufacturing Technology*, vol. 108, no. 7-8, pp. 2385–2396, 2020.

[6] R. J. Vikram, A. Singh, and S. Suwas, "Effect of heat treatment on the modification of microstructure of selective laser melted (SLM) IN718 and its consequences on mechanical behavior," *Journal of Materials Research*, vol. 35, no. 15, pp. 1949–1962, 2020.

[7] E. Pehlivan, J. Dugan, J. Fojt, S. Radek, R. Sylwia, and D. Matej, "Post-processing treatment impact on mechanical properties of SLM deposited Ti-6Al-4 V porous structure for biomedical application," *Materials*, vol. 13, pp. 1–11, 2020.

[8] L. Thijs, K. Kempen, J. P. Kruth, and J. V. Humbeeck, "Fine-structured aluminum products with controllable texture by selective laser melting of pre-alloyed AlSi10Mg powder," *Acta Materialia*, vol. 61, pp. 1809–1819, 2020.

[9] P. Krakhmalev, I. Yadroitsava, G. Fredriksson, and I. Yadroitsev, "In situ heat treatment in selective laser melted martensitic AISI 420 stainless steels," *Materials & Design*, vol. 87, pp. 380–385, 2016.

[10] S. Wen, S. Li, Q. Wei, C. Yan, Z. Sheng, and S. Yusheng, "Effect of molten pool boundaries on the mechanical properties of selective laser melting parts," *Journal of Materials Processing Technology*, vol. 214, pp. 2660–2667, 2014.

[11] O. O. Salman, C. Gammer, A. K. C. Haubey, J. Eckert, and S. Scudino, "Effect of heat treatment on microstructure and mechanical properties of 316L steel synthesized by selective laser melting," *Materials Science and Engineering*, vol. 748, pp. 205–212, 2014.

[12] D. Kong, C. Dong, X. Ni et al., "Mechanical properties and corrosion behavior of selective laser melted 316L stainless steel after different heat treatment processes," *Journal of Materials Science & Technology*, vol. 35, no. 7, pp. 1499–1507, 2019.

[13] E. Tascioglu, Y. Karabulut, and Y. Kaynak, "Influence of heat treatment temperature on the microstructural, mechanical, and wear behavior of 316L stainless steel fabricated by laser powder bed additive manufacturing," *International Journal of Advanced Manufacturing Technology*, vol. 107, pp. 1947–1956, 2020.

[14] Y. M. Wang, T. Voisin, T. Joseph et al., "Additively manufactured hierarchical stainless steel with high strength and ductility," *Nature Materials*, vol. 17, pp. 63–71, 2020.

[15] S. L. Sing, S. Huang, G. D. Goh et al., "Emerging metallic systems for additive manufacturing: in-situ alloying and multi-metal processing in laser powder bed fusion," *Progress in Materials Science*, vol. 119, Article ID 100795, 2021.

[16] Y. Qin, Q. Qi, P. Shi, P. J. Scott, and X. Jiang, "Automatic determination of part build orientation for laser powder bed fusion," *Virtual and Physical Prototyping*, vol. 16, no. 1, pp. 29–49, 2021.

[17] N. Nadammal, T. Mishurova, T. Fritsch et al., "Critical role of scan strategies on the development of microstructure, texture, and residual stresses during laser powder bed fusion additive manufacturing," *Additive Manufacturing*, vol. 38, Article ID 101792, 2020.

[18] H. A. Sheng, B. Rln, A. Jhkt, S. L. Sing, and W. Y. Yeong, "Resolving the porosity-unmelted inclusion dilemma during in-situ alloying of Ti34Nb via laser powder bed fusion," *Acta Materialia*, vol. 204, Article ID 116522, 2020.

[19] D. Ai, Y. Zhao, Q. Wang, and C. Li, "Experimental and numerical investigation of crack propagation and dynamic properties of rock in SHPB indirect tension test," *International Journal of Impact Engineering*, vol. 126, pp. 135–146, 2019.

[20] Q. Hu, Z. Feng, F. Hua, and F. Liu, "Dislocation density and mechanical threshold stress in OFHC copper subjected to SHPB loading and plate impact," *Materials Science and Engineering: A*, vol. 695, pp. 230–238, 2019.

[21] L. Guo, Y. Lv, Z. Deng, Y. Wang, and X. Zan, "Tension testing of silicone rubber at high strain rates," *Polymer Testing*, vol. 50, pp. 270–275, 2016.

[22] W. Shifeng, L. Shuai, W. Qingsong, C. Yan, Z. Sheng, and S. Yusheng, "Effect of molten pool boundaries on the mechanical properties of selective laser melting parts," *Journal of Materials Processing Technology*, vol. 214, no. 11, pp. 2660–2667, 2014.

[23] D. Kong, C. Dong, S. Wei et al., "About metastable cellular structure in additively manufactured austenitic stainless steels," *Additive Manufacturing*, vol. 38, Article ID 101804, 2021.

[24] K. Saeidi, X. Gao, Y. Zhong, and Z. J. Shen, "Hardened austenite steel with columnar sub-grain structure formed by laser melting," *Materials Science and Engineering: A*, vol. 625, pp. 221–229, 2015.

[25] I. A. Mbarek, R. Matadi Boumbimba, A. Rusinek, G. Z. Voyiadjis, P. Gerard, and A. Samadi-Dooki, "The dynamic behavior of poly (methyl methacrylate) based nano-rubbers subjected to impact and perforation: experimental investigations," *Mechanics of Materials*, vol. 122, pp. 9–25, 2018.

[26] L. Liu, Q. Ding, Y. Zhong et al., "Dislocation network in additive manufactured steel breaks strength-ductility trade-off," *Materials Today*, vol. 21, no. 4, pp. 354–361, 2018.

[27] Z. W. Chen, M. A. L. Phan, and K. Darvish, "Grain growth during selective laser melting of a Co-Cr-Mo alloy," *Journal of Materials Science*, vol. 52, no. 12, pp. 7415–7427, 2017.

[28] M. S. Pham, B. Dovgyy, P. A. Hooper, C. M Gourlay, and A Piglione, "The role of side-branching in microstructure development in laser powder-bed fusion," *Nature Communications*, vol. 11, no. 749, p. 749, 2020.

[29] D. Kong, X. Ni, C. Dong et al., "Anisotropy in the microstructure and mechanical property for the bulk and porous 316L stainless steel fabricated via selective laser melting," *Materials Letters*, vol. 235, pp. 1–5, 2019.

[30] D. Kong, C. Dong, X. Ni et al., "The passivity of selective laser melted 316L stainless steel," *Applied Surface Science*, vol. 504, Article ID 144495, 2020.

[31] H. Guo, W. Guo, A. V. Amirkhizi, R. Zou, and K. Yuan, "Experimental investigation and modeling of mechanical behaviors of polyurea over wide ranges of strain rates and temperatures," *Polymer Testing*, vol. 53, pp. 234–244, 2016.

[32] J. Chen, H. Wei, K. Bao et al., "Dynamic mechanical properties of 316L stainless steel fabricated by an additive manufacturing process," *Journal of Materials Research and Technology*, vol. 11, pp. 170–179, 2016.

[33] B. Song, E. Nishida, B. Sanborn et al., "Compressive and tensile stress-strain responses of additively manufactured (AM) 304L stainless steel at high strain rates," *Journal of Dynamic Behavior of Materials*, vol. 3, no. 3, pp. 412–425, 2017.

[34] J. G. Song, J. B. Seol, J. M. Park, S. Hyokyung, P. Sun Hong, and K. Hyoung Seop, "Effects of cell network structure on the

strength of additively manufactured stainless steels," *Metals and Materials International*, vol. 27, 2021.

[35] W. S. Shin, B. Son, W. Song et al., "Heat treatment effect on the microstructure, mechanical properties, and wear behaviors of stainless steel 316L prepared via selective laser melting," *Materials Science and Engineering: A*, vol. 806, Article ID 140805, 2021.

[36] S. Zhang, M. C. Gong, X. Y. Zeng, and M. Gao, "Residual stress and tensile anisotropy of hybrid wire arc additive-milling subtractive manufacturing," *Journal of Materials Processing Technology*, vol. 293, Article ID 117077, 2021.

[37] P. F. Li, Y. D. Gong, X. L. Wen, Bo Xin, Y. Liu, and S. Qu, "Surface residual stresses in additive/subtractive manufacturing and electrochemical corrosion," *International Journal of Advanced Manufacturing Technology*, vol. 98, pp. 287–297, 2018.

[38] X. Cui, S. Zhang, C. Wang, C. H. Zhang, J. Chen, and J. B. Zhang, "Effects of stress-relief heat treatment on the microstructure and fatigue property of a laser additive manufactured 12CrNi2 low alloy steel," *Materials Science and Engineering: A*, vol. 791, Article ID 139738, 2020.

[39] A. M. Bandar, P. Vo, R. Mongrain, E. Irissou, and S. Yue, "Effect of heat treatment on the microstructure and mechanical properties of stainless steel 316L coatings produced by cold spray for biomedical applications," *Journal of Thermal Spray Technology*, vol. 23, pp. 641–652, 2019.